The Asymmetric Schrock Olefin Metathesis Catalyst. A Computational Study

T. P. M. Goumans, Andreas W. Ehlers, and Koop Lammertsma*

Department of Organic and Inorganic Chemistry, Faculty of Sciences, Vrije Universiteit, De Boelelaan 1083, NL-1081 HV, Amsterdam, The Netherlands

Received February 16, 2005

The mechanism of the transition metal catalyzed olefin metathesis reaction with the Schrock catalyst is investigated with pure (BP86) and hybrid (B3LYP) density functional theory. On the free-energy surface there is no adduct between ethylene and model catalyst $(MeO)_2Mo(CH_2)NH$ but instead a single transition on a flat surface giving a metallacyclobutane with a trigonal bipyramidal conformation that has a sizable barrier for conversion to the square pyramidal form. The model was expanded to the active asymmetric Schrock catalyst and investigated with QM/MM, using BP86 for the QM part and AMBER 95 for the MM part, for the experimentally known ring-closing metathesis of a symmetrical triene. The factors effecting chiral induction to the observed product are delineated.

Introduction

Transition metal catalyzed olefin metathesis has become an increasingly indispensable tool in organic chemistry over the past decade with extensive applications ranging from the synthesis of macrocylic rings to olefin polymerization.[1] The success of this relatively young reaction is due to the rapid developments in homogeneous catalysts, of which two types dominate, the Schrock's molybdenum-based (**A**)[1c,f,2] and the Grubbs' ruthenium-based ones (**B**)[1b,e,3] (Figure 1). Schrock catalyst **A** is generally more active, while the "first-generation" Grubbs catalyst (**B**, L = PR_3) tends to have a higher functional-group tolerance and is more robust, but the second-generation Grubbs catalysts (**B**, L = N-heterocyclic carbene) have activities similar to that of the Schrock catalyst.[4]

The generally accepted mechanism for olefin metathesis, first proposed by Chauvin,[5] involves the formation of a metallacyclobutane, either as an intermediate or as a transition structure (Scheme 1). This process has been thoroughly investigated experimentally for both the molybdenum-based[1c,f,6] and ruthenium-based catalysts.[1b,e,7] Both types of catalysts have also been the subject of computational studies.[8,9]

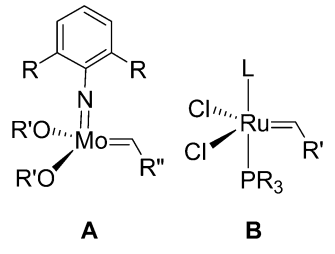

Figure 1. Metathesis catalysts.

Scheme 1. Chauvin Mechanism for Olefin Metathesis

Asymmetric catalysis is an important and rapidly expanding research area.[10] The aim of asymmetric catalysis is the cheap, efficient, and fast synthesis of

* To whom correspondence should be addressed. E-mail: lammert@chem.vu.nl.

(1) Recent reviews on the metathesis reaction: (a) Ivan, K. J.; Mol, J. C. *Olefin Metathesis and Metathesis Polymerization*; Academic Press: San Diego, 1997. (b) Grubbs, R. H.; Chang, S. *Tetrahedron* **1998**, *54*, 4413−4450. (c) Schrock, R. R. *Tetrahedron* **1999**, *55*, 8141−8153. (d) Fürstner, A. *Angew. Chem.* **2000**, *112*, 3140−3172; *Angew. Chem., Int. Ed.* **2000**, *39*, 3012−3043. (e) Trnka, T. M.; Grubbs, R. H. *Acc. Chem. Res.* **2001**, *34*, 18−29. (f) Schrock, R. R.; Hoveyda, A. H. *Angew. Chem.* **2003**, *115*, 4740−4782; *Angew. Chem., Int. Ed.* **2003**, *42*, 4592−4633.

(2) (a) Feldman, J.; Murdzek, J. S.; Davis, W. M.; Schrock, R. R. *Organometallics* **1989**, *8*, 2260−2265. (b) Bazan, G. C.; Khosravie, E.; Schrock, R. R.; Feast, W. J.; Gibson, V. C.; Oregan; M. B.; Thomas, J. K.; Davis, W. M. *J. Am. Chem. Soc.* **1990**, *112*, 8378−8387. (c) Schrock, R. R.; Murdzek, J. S.; Bazan, G. C.; Robbins, J.; DiMare, M.; O'Regan, M. *J. Am. Chem. Soc.* **1990**, *112*, 3875−3886. (d) Oskam, J. H.; Fox, H. H.; Yap, K. B.; McConville, D. H.; O'Dell, R.; Lichtenstein, B. J.; Schrock, R. R. *J. Organomet. Chem.* **1993**, *459*, 185−198.

(3) (a) Nguyen, S. T.; Johnson, L. K.; Grubbs, R. H.; Ziller, J. W. *J. Am. Chem. Soc.* **1992**, *114*, 3974−3975. (b) Nguyen, S. T.; Grubbs, R. H.; Ziller, J. W. *J. Am. Chem. Soc.* **1993**, *115*, 9858−9859. (c) Schwab, P.; France, M. B.; Ziller, J. W.; Grubbs, R. H. *Angew. Chem.* **1995**, *107*, 2179−2181; *Angew. Chem., Int. Ed.* **1995**, *34*, 2039−2041. (d) Wu, Z.; Nguyen, S. T.; Grubbs, R. H.; Ziller, J. W. *J. Am. Chem. Soc.* **1995**, *117*, 5503−5511. (e) Schwab, P.; Grubbs, R. H.; Ziller, J. W. *J. Am. Chem. Soc*. **1996**, *118*, 100−110.

(4) (a) Scholl, M.; Ding, S.; Lee, C. W.; Grubbs, R. H. *Org. Lett.* **1999**, *1*, 953−956. (b) Chatterjee, A. K.; Grubbs, R. H. *Org. Lett.* **1999**, *1*, 1751−1753. (c) Scholl, M.; Trnka, T. Morgan J. P.; Grubbs R. H. *Tetrahedron Lett.* **1999**, *40*, 2247−2250. (d) Huang, J.; Stevens, E. D.; Nolan, S. P.; Peterson, J. L. *J. Am. Chem. Soc.* **1999**, *121*, 2674−2678. (e) Morgan, J. P.; Grubbs, R. H. *Org. Lett.* **2000**, *2*, 3153−3155. (f) Fürstner, A.; Ackermann, L.; Gabor, B.; Goddard, R.; Lehmann, C. W.; Mynott, R.; Stelzer, F.; Thiel, O. R. *Chem. Eur. J.* **2001**, *7*, 3236−3253.

(5) Hérrison, J. L.; Chauvin, Y. *Makromol. Chem.* **1971**, *141*, 161−176.

(6) (a) Schrock, R. R.; DePue, R.; Feldman, J.; Schaverien, C. J.; Dewan, J. C.; Liu, A. H. *J. Am. Chem. Soc.* **1988**, *110*, 1423−1435. (b) Feldman, J.; Davis, W. M.; Thomas, J. K.; Schrock, R. R. *Organometallics* **1990**, *9*, 2535−2548. (c) Feldman, J.; Schrock, R. R. *Prog. Inorg. Chem.* **1991**, *39*, 1−74. (d) Oskam, J. H.; Schrock, R. R. *J. Am. Chem. Soc.* **1993**, *115*, 11831−11845.

10.1021/om050109l CCC: $30.25
Publication on Web 05/18/2005

chiral compounds for pharmaceutical and agricultural applications. Natural product syntheses that frequently apply a metathesis step could benefit greatly from the development of enantioselective catalysts.[11] A better mechanistic understanding might facilitate the rational design of the required enantioselective catalysts, a process to which this paper makes a contribution. Because of the sheer size of the catalyst, the use of a hybrid QM/MM method is desired in which the quantum mechanical (QM) part treats the electronic interactions, while molecular mechanics (MM) is used for the steric bulk. Such a study addressed recently the mechanism by which asymmetric Grubbs catalyst **C** induces chirality.[12] The phenyl groups at the two chiral carbons of the heterocyclic carbene were found to invoke chiral twisting of the substituted N-bonded aryl rings, creating a chiral pocket around the ruthenium−carbene bond, which induces enantioface selection in the ring-closing step.

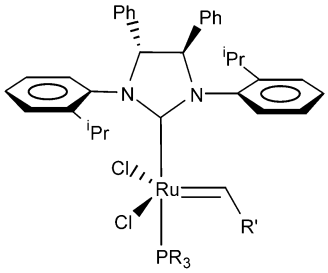

C

In the present computational study we investigate the origin of chiral induction for the enantioselective Schrock metathesis catalyst that was developed recently.[11a]

Computational Details

All hybrid density functional theory calculations (B3LYP)[13] were performed with the Gaussian suite of programs,[14] using the LANL2DZ basis and pseudopotentials[15] on molybdenum, and the 6-31G** basis for all other atoms. All pure DFT calculations have been performed with the parallelized ADF suite of programs, releases 2000.02 and 2002.01.[16] Geometry optimizations were carried out with the generalized gradient approximation, using nonlocal corrections to exchange by Becke[17] and to correlation by Perdew[18] (BP86), including relativistic effects with the Zeroth Order Regular Approximation (ZORA).[19] The Kohn−Sham MOs were expanded in a large, uncontracted basis set of Slater-type orbitals (STOs), of a triple-ζ + polarization functions quality (ADF basis set IV or TZP). The [He]-cores of carbon and oxygen were treated by the frozen-core approximation. Molybdenum was described by a frozen [Zn]-core, a double-ζ 4s-shell, triple-ζ 4p-, 5s-, and 4d-shells, and a 5p-polarization function. An auxiliary set of STOs was used to fit the density for the Coulomb-type integrals.[16a] Thermal energy corrections and standard entropies are computed from unscaled harmonic frequencies at 298.15 K. The nature of all transition states and intermediates was confirmed with frequency calculations. Intrinsic reaction coordinate (IRC) calculations were unfortunately not successful for the early transition states (**$TS_{1\rightarrow2}$**, vide infra), due to the flatness of the potential energy surface, but the transition vectors would correspond in each case to the expected reaction coordinate. QM/MM[20] calculations were performed with ADF using the DFT approach for the QM system and a modified AMBER95 force field for the MM part.[21] The partitioning between the two parts is complex, as it involves chemical bonds, which as a consequence gives an unsaturated QM fragment. There are two general approaches for satisfying the valency of the unsaturated bond,[22] the hybrid-orbital methods, pioneered by Warshell and Levitt,[20a] and the link-atom or

(7) (a) Dias, E. L.; Nguyen, S. T.; Grubbs, R. H. *J. Am. Chem. Soc.* **1997**, *119*, 3887−3897. (b) Ulman, M.; Grubbs, R. H. *Organometallics* **1998**, *12*, 2484−2489. (c) Sanford, M. S.; Ulman, M.; Grubbs, R. H. *J. Am. Chem. Soc.* **2001**, *123*, 749−750. (d) Sanford, M. S.; Love, J. A.; Grubbs, R. H. *J. Am. Chem. Soc.* **2001**, *123*, 6543−6554. (e) Love, J. A.; Sanford, M. S.; Day, M. W.; Grubbs, R. H. *J. Am. Chem. Soc.* **2003**, *125*, 10103−10109.

(8) Schrock-type catalysts: (a) Folga, E.; Ziegler, T. *Organometallics* **1993**, *12*, 325−337. (b) Monteyne, K.; Ziegler, T. *Organometallics* **1998**, *17*, 5901−5907. (c) Wu, Y.-D.; Peng, Z.-H. *J. Am. Chem. Soc.* **1997**, *119*, 8043−8049.

(9) Grubbs-type catalysts: (a) Aagard, O. M.; Meier, R. J.; Buda, F. *J. Am. Chem. Soc.* **1998**, *120*, 7174−7182. (b) Weskamp, T.; Kohl, F. J.; Hieringer, W.; Gleich, D.; Herrmann, W. A. *Angew. Chem.* **1999**, *111*, 2573−2578; *Angew. Chem., Int. Ed.* **1999**, *38*, 2416−2419. (c) Adlhart, C.; Hinderling, C.; Baumann, H.; Chen, P. *J. Am. Chem. Soc.* **2000**, *122*, 8204−8214. (d) Cavallo, L. *J. Am. Chem. Soc.* **2002**, *124*, 8965−8973. (e) Adlhart, C.; Chen, P. *Angew. Chem.* **2002**, *114*, 4668−4671; *Angew. Chem., Int. Ed.* **2002**, *41*, 4484−4487. (f) Vyboischikov, S. F.; Bühl, M.; Thiel, W. *Chem. Eur. J.* **2002**, *8*, 3962−3975. (g) Fomine, S.; Vargas, S. M.; Tlenkopatchev, M. A. *Organometallics* **2003**, *22*, 93−99. (h) Adlhart, C.; Chen, P. *J. Am. Chem. Soc.* **2004**, *126*, 3496−3510.

(10) (a) Trost, B. M. *PNAS* **2004**, *101*, 5348−5355. (b) Knowles, W. S. *Angew. Chem., Int. Ed.* **2002**, *41*, 1998−2007. (c) Noyori, R. *Angew. Chem., Int. Ed.* **2002**, *41*, 2008−2022. (d) Sharpless, B. *Angew. Chem., Int. Ed.* **2002**, *41*, 2024−2032.

(11) (a) Hoveyda, A. H.; Schrock, R. R. *Chem. Eur. J.* **2001**, *7*, 945−950. (b) Seiders, T. J.; Ward, W. D.; Grubbs, R. H. *Org. Lett.* **2001**, *3*, 3225−3228. (c) Schrock, R. R.; Jamieson, J. Y.; Dolman, S. J.; Miller, S. A.; Bonitatebus, P. J., Jr.; Hoveyda, A. H. *Organometallics* **2002**, *21*, 409−417. (d) van Veldhuizen, J. J.; Gillingham, D. G.; Garber, S. B.; Kataoka, O.; Hoveyda, A. H. *J. Am. Chem. Soc.* **2003**, *125*, 12502−12508.

(12) Costabile, C.; Cavallo, L. *J. Am. Chem. Soc.* **2004**, *126*, 9592−9600.

(13) (a) Becke, A. D. *J. Chem. Phys.* **1993**, *98*, 5648−5652. (b) Lee, C.; Yang, W.; Parr, R. G. *Phys. Rev. B* **1988**, *37*, 785−789. (c) Stephens, P. J.; Devlin F. J.; Chabaloski, C. F.; Frisch M. A. *J. Phys. Chem.* **1994**, *98*, 11623−11627.

(14) Frisch, M. J.; Trucks, G. W.; Schlegel, H. B.; Scuseria, G. E.; Robb, M. A.; Cheeseman, J. R.; Zakrzewski, V. G.; Montgomery, J. A., Jr.; Stratmann, R. E.; Burant, J. C.; Dapprich, S.; Millam, J. M.; Daniels, A. D.; Kudin, K. N.; Strain, M. C.; Farkas, O.; Tomasi, J.; Barone, V.; Cossi, M.; Cammi, R.; Mennucci, B.; Pomelli, C.; Adamo, C.; Clifford, S.; Ochterski, J.; Petersson, G. A.; Ayala, P. Y.; Cui, Q.; Morokuma, K.; Malick, D. K.; Rabuck, A. D.; Raghavachari, K.; Foresman, J. B.; Cioslowski, J.; Ortiz, J. V.; Baboul, A. G.; Stefanov, B. B.; Liu, G.; Liashenko, A.; Piskorz, P.; Komaromi, I.; Gomperts, R.; Martin, R. L.; Fox, D. J.; Keith, T.; Al-Laham, M. A.; Peng, C. Y.; Nanayakkara, A.; Gonzalez, C.; Challacombe, M.; Gill, P. M. W.; Johnson, B.; Chen, W.; Wong, M. W.; Andres, J. L.; Gonzalez, C.; Head-Gordon, M.; Replogle, E. S.; Pople, J. A. *Gaussian 98*, Revision A.7; Gaussian, Inc.: Pittsburgh, PA, 1998.

(15) Hay, P. J.; Wadt, W. R. *J. Chem. Phys.* **1985**, *82*, 270−283.

(16) (a) Baerends, E. J.; Ellis, D. E.; Ros, P. *Chem. Phys.* **1973**, *2*, 41−51. (b) te Velde, G.; Baerends, E. J. *J. Comput. Phys.* **1992**, *99*, 84−98. (c) Fonseca-Guerra, C.; Visser, O.; Snijders, J. G.; te Velde, G.; Baerends, E. J. In *METECC-95*, Clementie, E., Corongiu, C., Eds.; Cagliari, 1995; pp 303−395. (d) te Velde, G.; Bickelhaupt, F. M.; Baerends, E. J.; Fonseca-Guerra, C.; van Gisbergen, S. J. A.; Snijders, J. G.; Ziegler, T. *J. Comput. Chem.* **2001**, *22*, 931−967.

(17) Becke, A. D. *Phys. Rev. A* **1988**, *38*, 3098−3100.

(18) Perdew, J. P. *Phys. Rev. B* **1986**, *33*, 8822−8824.

(19) van Lenthe, E.; Ehlers, A. W.; Baerends, E. J. *J. Chem. Phys.* **1999**, *110*, 8943−8953.

(20) (a) Warshell, A.; Levitt, M. *J. Mol. Biol.* **1976**, *103*, 227−249. (b) Singh, U. C.; Kollman, P. A. *J. Comput. Chem.* **1986**, *7*, 718−730. (c) Field, M. J.; Bash, P. A.; Karplus, M. *J. Comput. Chem.* **1990**, *11*, 700−733. (d) Gao, J. *Rev. Comput. Chem.* **1996**, *7*, 119−185.

(21) (a) AMBER95: Cornell, W. D.; Cieplak, P.; Bayly, C. I.; Gould, I. R.; Merz, K. M.; Ferguson, D. M., Spellmeyer, D. C.; Fox, T.; Caldwell, J. W., Kollmann, P. A. *J. Am. Chem. Soc.* **1995**, *117*, 5179−5197. (b) Additions to the force field (in units as in ADF's AMBER95.ff): Cl, Mo, and Ru van der Waals parameters from UFF: Rappé, A. K.; Casewit, C. J.; Colwell, K. S.; Goddard, W. A., III; Skiff, W. M. *J. Am. Chem. Soc.* **1992**, *114*, 10024−10035. (c) QM/MM parameters for Schrock catalysts: bond distance ratio of MM atoms to capping atoms (H): OS−CA/OS−H 1.441, N*−CA/N*−H 1.3484. Additions to the force field: angle bending: $k_{N^*-CA-CA} = 160$, $\theta_{N^*-CA-CA} = 120$, $k_{CA-CA-N^*} = 126$, $k_{OS-CA-CA\ S} = 85.35$, $\theta_{OS-CA-CA} = 120$; torsion: $k_{Mo-OS-CA-CA}$, $k_{Mo-N^*-CA-CA} = 0.383$ (periodicity 3).

(22) For a recent review on these two methodologies, see: Amara, P.; Field, M. J. *Theor. Chem. Acc.* **2003**, *109*, 43−52.

Scheme 2. Degenerate Olefin Metathesis with a Model Schrock-Type Catalyst

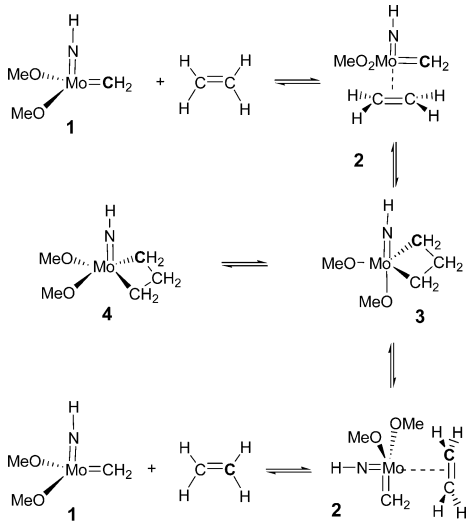

capping-atom methods, pioneered by Singh and Kollman.[20b] We use the modified IMOMM approach as implemented in ADF,[23] which is based on the link-atom method using hydrogen as capping atom.

Results and Discussion

The first part of the discussion concerns the interaction between ethylene and the simplified model Schrock-type catalyst $(MeO)_2Mo(CH_2)NH$ (**1**) to establish the general outline for the mechanism of the metathesis process. In the second part the simple model is expanded to asymmetric catalyst **A** to explore the enantioselective pathways.

Olefin Metathesis. For the simplified catalyst **1** the metathesis is a degenerate process for symmetry reasons, where the addition of ethylene to form metallacycle **3** is identical to the expulsion of the olefin (Scheme 2). Metathesis can take place either directly from the trigonal bipyramidal conformation (TBP) **3** of the metallacyclobutane or via the more stable square pyramidal (SQP) conformation **4**. The intermediacy of a (short-lived) olefin adduct was found by Anslyn and Grubbs[24] to agree with the kinetics of the cycloreversal of titanium metallacycles. However, generalized valence bond calculations by Upton and Rappé could not locate such an olefin methylidene complex and suggested the metathesis to occur instead in a single step.[25]

Both Ziegler et al. (BP86)[8a,b] and Wu and Peng (B3LYP)[8c] predicted a single transition state for the addition reaction, but with different geometries. In the metathesis with the $Cl_2OMo{=}CH_2$ model,[8a,b] Ziegler, using BP86/TZ2P,[26] found a very *early* transition state (**TS$_{1\to2}$**) on the ethylene addition trajectory (σ-bond forming distances Mo−C 3.09 Å and C−C 3.20 Å), with a low barrier of 4.7 kcal/mol. Wu and Peng, on the other hand, using B3LYP/DZP[27] for model **1** (OCF_3 and OMe),[8c] found a very *late* transition structure (**TS$_{2\to3}$**, σ-bond forming distances of ca. 2.5 Å), with a barrier that is low (OMe, 4.8 kcal/mol) or even negative (OCF_3, −2.6 kcal/mol). Both the early (Ziegler) and late (Wu and Peng) transitions would coexist if it concerns a two-step mechanism with a small barrier for ethylene coordination and a small barrier for metallacyclobutane formation. Both theoretical studies indicate a rate-determining cycloreversal step for the metathesis of sterically uncongested substrates and catalysts.

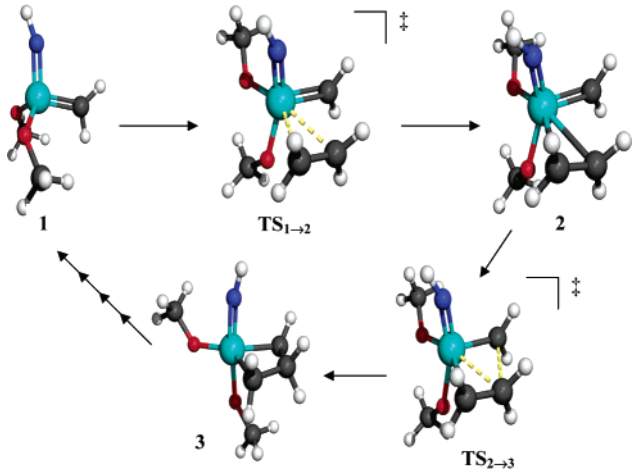

Figure 2. Calculated structures along Mo-catalyzed olefin metathesis pathway (BP86).

Table 1. Calculated BP86 and B3LYP Metathesis Distances of 1 (Å)

$MeO_2Mo{=}C_1$ $C_2{=}C_3$	Mo-C_1		Mo-C_2		C_1-C_3		C_2-C_3	
	BP86	B3LYP	BP86	B3LYP	BP86	B3LYP	BP86	B3LYP
1 + $H_2C{=}CH_2$	1.908	1.892					1.334	1.331
TS$_{1\to2}$	1.918	1.902	3.417	3.387	3.573	3.592	1.337	1.336
2	1.944	1.912	2.454	2.726	2.606	2.983	1.378	1.351
TS$_{2\to3}$	1.950	1.941	2.402	2.360	2.489	2.337	1.388	1.398
3	2.106	2.083	2.106	2.083	1.593	1.595	1.593	1.595

Table 2. Relative BP86 and B3LYP Energies (kcal/mol) along the Mo-Catalyzed Metathesis Pathway

molecule	E_{BP}	$G^{298}{}_{BP}$	E_{B3LYP}	$G^{298}{}_{B3LYP}$
1 + $H_2C{=}CH_2$	0.0	0.0	0.0	0.0
TS$_{1\to2}$	3.5	14.9	2.9	14.3
2	−0.4	15.6	1.3	15.2
TS$_{2\to3}$	−0.2	15.5	3.0	19.1
3	−12.0	7.6	−8.4	8.8
TS$_{3\to4}$	−1.8	15.6	3.1	20.1
4	−19.8	−2.2	−17.9	−2.1

One- or Two-Step Mechanism? We studied the mechanism for the degenerate olefin metathesis reaction at both the BP86/TZP and B3LYP/DZP levels of theory. The stationary points are shown in Figure 2, and the bond lengths pertaining to the metathesis process are given in Table 1. The relative energies are listed in Table 2 and are graphically displayed in Figure 3. Three stationary points were located both at BP86 and at B3LYP, that is, an early (**TS$_{1\to2}$**) and a late (**TS$_{2\to3}$**) transition structure and the intermediate ethylene adduct (Figure 2).

The incoming ethylene distorts the tetrahedral geometry of the molybdenum carbene to facilitate side-on

(23) (a) Maseras, F.; Morokuma, K. *J. Comput. Chem.* **1995**, *9*, 1170−1179. (b) Woo, T. K.; Cavallo, L.; Ziegler, T. *Theor. Chem. Acc.* **1998**, *100*, 307−313.

(24) Anslyn, E. V.; Grubbs, R. H. *J. Am. Chem. Soc.* **1987**, *109*, 4880−4890.

(25) Upton, T. H.; Rappé, A. K. *J. Am. Chem. Soc.* **1985**, *107*, 1206−1218.

(26) Using two polarization functions (basis set V or TZ2P) and a quasi-relativistic approach instead of ZORA.

(27) Using an extra d-polarization function on the LANL2DZ ECP and 6-31G* for all other elements.

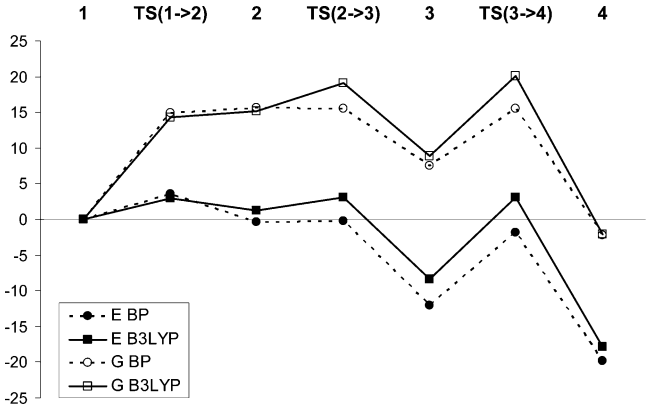

Figure 3. Relative energies (E, solid points) and Gibbs free energies (G, open points) calculated at BP86 (dotted lines, circles) and B3LYP (solid lines, squares) for the Mo-catalyzed olefin metathesis of **1** and ethylene (in kcal/mol).

coordination, which is associated with a small barrier for the near isothermic formation of the ethylene adduct. In this adduct the bond lengths are little perturbed. Bond formation is slightly more advanced for the BP86 than for the B3LYP structure (Table 2). This is reflected in the slight stabilization of the adduct at BP86 and the similar destabilization with respect to the starting material at B3LYP, but the differences are within the margins of error. The bonds are developed in transition structure $\mathbf{TS_{2\rightarrow 3}}$ for converting the ethylene adduct into the metallacycle, but the C−C σ-bonds are still far from their equilibrium distance. Also the barrier for this second step is very small (BP86 0.2; B3LYP 1. 8 kcal/mol), which underscores that the hypersurface for forming the metallocycle is very flat. On this path (**1** → **3**), the olefin C=C and methylene Mo=C bonds increase in length with the concurrent formation of the C−C and Mo−C bonds in an asynchronous manner.

Free-Energy Surface. Entropy factors should influence the hypersurface because the number of particles changes during the metathesis.[28] To evaluate this effect, we calculated the free energies of the stationary points (Table 2, Figure 3). There are two important effects; namely, **3** is formed in a single step that has become endergonic. The endergonicity for forming **3** is a direct consequence of the cyclization reaction, which is already evident on coordinating ethylene to the catalyst. The change in the nature of the reaction coordinate is more subtle. With BP86 ethylene adduct **2** has become less stable than both the transition structures $\mathbf{TS_{1\rightarrow 2}}$ and $\mathbf{TS_{2\rightarrow 3}}$, but the free energy differences are within 0.5 kcal/mol, which is well within the error limits. Clearly the formation of metallocycle **3** occurs on a very flat free-energy surface at this level of theory. With B3LYP $\mathbf{TS_{2\rightarrow 3}}$ remains the transition for formation of the metallacycle, but there is no longer an intermediate adduct; adduct **2** is less stable than $\mathbf{TS_{1\rightarrow 2}}$ albeit by only 0.1 kcal/mol. Thus, with B3LYP a late transition is associated with the formation of **3**.

Converting trigonal bipyramidal **3** to the square pyramidal conformation **4** is a favorable process (Table 2, Figure 3) with a (free) energy barrier that is of the same magnitude as that for the formation of **3** ($\mathbf{TS_{2\rightarrow 3}}$) both at BP86 and at B3LYP. In fact, its formation from ethylene and the catalyst is even slightly favored (2 kcal/mol) at the free-energy surface.

Scheme 3. Catalytic Desymmetrization of a Prochiral Triolefin

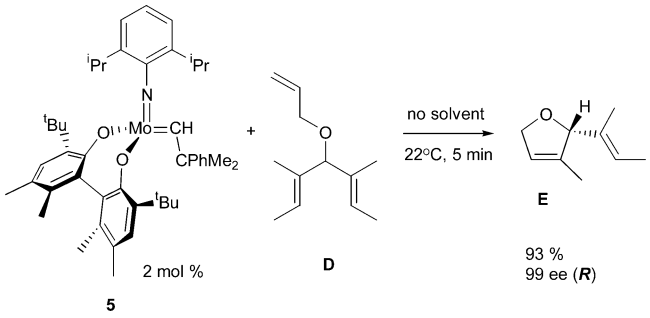

Asymmetric Catalysis. Asymmetric molybdenum catalyst **5**, with the same framework as model **1** expanded with large substituents and chiral centers, has been shown to desymmetrize prochiral olefin **D** under mild reaction conditions to give ring-closing metathesis product *R*-**E** in high yield and high enantiomeric excess (Scheme 3).[11a] To explore the mechanism of asymmetric induction by this potent enantioselective catalyst, we investigated the catalytic pathway for the reported asymmetric RCM of achiral triene ether **D** with the QM/MM methodology.

The mechanistic scheme we considered for formation of heterocycle **E** is shown in Figure 4. For effective ring-closing metathesis to take place, the unsubstituted double bond of triene **D** must react first with catalyst **5** (or the related **5′**, vide infra) to give intermediate **7** via metallacycle **6**. Enantioface selection occurs in the subsequent rate-determining ring-closing step **7** → **8**, as ring-opening from trigonal bipyramidal **8** to yield the chiral *R*-1,4-dihydrofuran **E** (and asymmetric catalyst **5′**) is the faster process (vide supra).

To analyze in more detail the enantioselective step that results in chiral induction, we examined the trigonal bipyramidal and square pyramidal metallacyclobutanes **8** and **9**, respectively. In our model the aryl rings and their substituents are included in the force field (MM) component, while the molybdenum, oxygen, and nitrogen atoms and the triolefin are part of the DFT component (see Figure 5). This choice was justified by QM calculations on a smaller test system that showed neither agostic nor other significant electronic interactions of the spectator ligands.

There are two possible isomers of carbene complex **7**, one with the carbenic substituent *anti* to the imido group and the other with a *syn* orientation. The *anti*-isomer is favored over the *syn* form by 5.5 kcal/mol. Interconversion of the two isomers is facile with a *syn* → *anti* barrier of 10−13 kcal/mol.[6d,8c] Ring closing of carbene **7** to trigonal bipyramidal metallacycle **8** can then result in 16 possible isomers due to four stereogenic centers (2^4), namely, (1) the carbenic substituent that is either *syn* or *anti*, (2) ring-closure by either front- or backside attack, (3) *cis*- or *trans*-fusion of the metallacyclobutane and tetrahydrofuran, and (4) the desymmetrized carbon center acquires an *R*- or *S*-configuration. These possibilities are displayed in Figure 6. Because *trans*-fusion of the molybdacyclobutane with the tetrahydrofuran ring is unfavorable with respect to

(28) Carreón-Macedo, J.-L.; Harvey, J. N. *J. Am. Chem. Soc.* **2004**, *126*, 5789−5797.

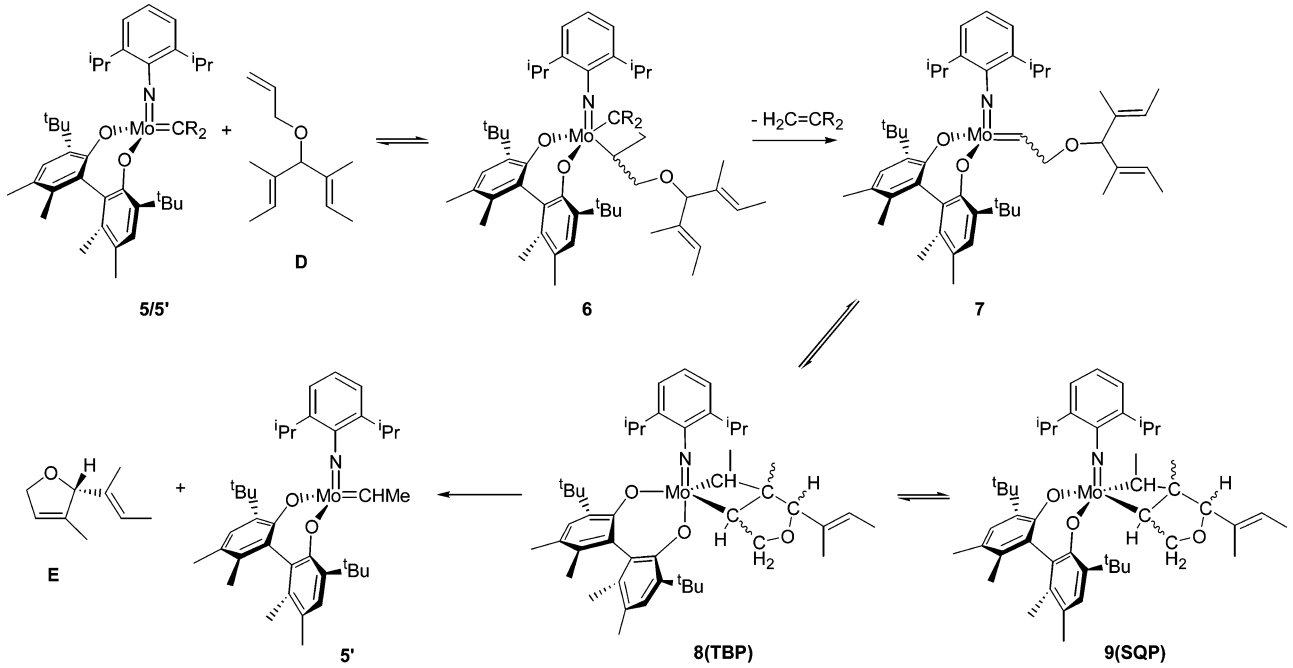

Figure 4. Desymmetrization of prochiral triolefin **D** by ring-closing metathesis with Schrock catalyst **5**.

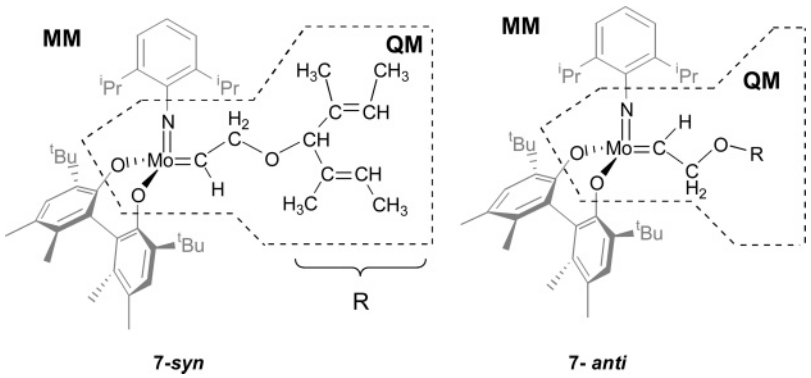

Figure 5. QM/MM partitioning of intermediate **7** during ring-closing desymmetrization. The QM atoms are in black, and the MM atoms are in gray.

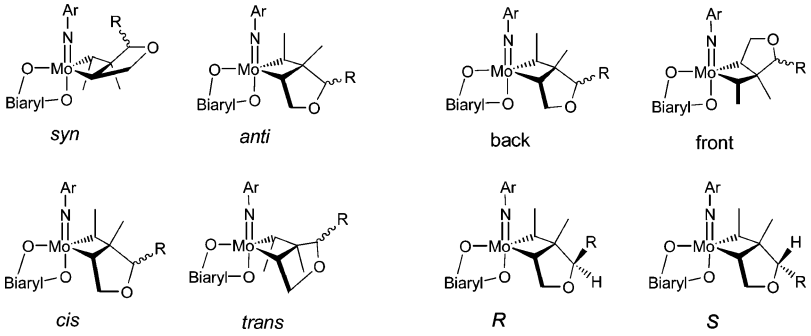

Figure 6. Stereogenic centers and their relative conformations in bicyclic intermediates of asymmetric ring-closing metathesis with catalyst **5**.

cis-fusion, we reduced the set of isomers to eight (2^3) by considering only *cis*-fusion.[29] The relative energies of these eight isomers of **8** together with those of the isomeric square pyramidal metallacycles **9** are listed in Table 3.

We assume the intramolecular ring closure of **7** that results in the trigonal bipyramidal metallacycle to occur in a manner similar to that discussed for model catalyst **1**, that is, in a single step without intermediates. Indeed, in selected searches we were unable to locate ethylene adducts. Unfortunately, we could neither locate transition structures for the ring-opening/closing steps because of the flatness of the potential energy surface. Rigorous searches through frequency calculations that are commonly applied by QM methods to locate transi-

(29) For example, the lowest energy *trans*-fused TBP metallacycle isomer, *cis*-**8**-back-*anti*-*R*, is 24.2 kcal/mol less stable than the *cis*-fused isomer; the energe difference with respect to **7**-*anti* amounts to 29.5 kcal/mol. The *trans* isomers of various SQP isomers **9** are >10 kcal/mol less stable than the *cis* isomers.

Table 3. Relative IMOMM Energies for the Ring-Closing Metathesis Desymmetrization (in kcal/mol)[a]

molecule	*R*	*S*
7-*anti*	0	
7-*syn*	5.5	
8-back-*anti*	5.0	9.7
8-back-*syn*	29.4	19.9
8-front-*anti*	22.9	20.3
8-front-*syn*	5.2	8.0
9-back-*anti*	4.2	4.7
9-back-*syn*	4.8	2.3
9-front-*anti*	1.5	−0.3
9-front-*syn*	10.9	2.9
products	3.2	

[a] See Figure 6 for the denomenation of the stereogenic centers.

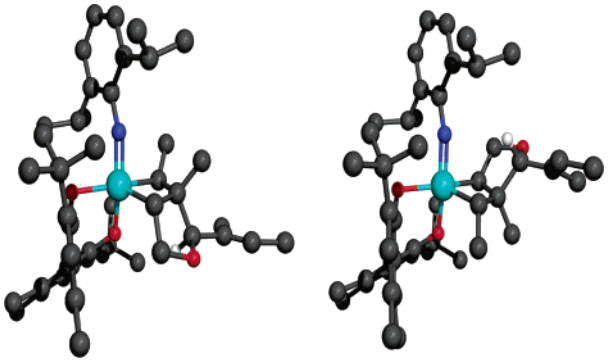

Figure 7. Calculated IMOMM structures of **8**-back-*anti*-*R* (left) and **8**-front-*syn*-*R* (right).

tion structures were not feasible within the IMOMM scheme due to the extreme demand on computer resources. From the relative energies of the transition states the enantiomeric excess could have been determined directly.[30] Instead, we use the reaction energies for formation of **8** from **7**, which should follow the same trend as the activation energies assuming that the Bell−Evans−Polanyi principle applies.[31]

The most stable and of nearly equal energy isomers that result from ring closure, **8**-back-*anti* and **8**-front-*syn* (Figure 7), both favor an *R*- over an *S*-configuration by 4.7 and 2.8 kcal/mol, respectively; the *R* and *S* forms of both the back-*syn* and front-*anti* isomers are much higher in energy (Table 3). Formation of **8**-front-*syn*-*R* from **7**-*syn*, which is the less stable carbene isomer, is virtually thermoneutral (−0.27 kcal/mol), while that for generating the favored **8**-back-*anti*-*R* form (by 0.2 kcal/mol) from **7**-*anti*, which is the more stable carbene isomer, is endothermic, but by only 5.02 kcal/mol. If the barrier for Mo=C isomerization (10−13 kcal/mol)[6d,8c] is smaller than that for ring closure, isomers **7**-*syn* and **7**-*anti* are likely to interchange. Applying the Curtin−Hammett postulate[32] to distinguish between the formation of the energetically most favored *R* and *S* forms of **8**, which are the conversion of **7**-*anti* and **7**-*syn* into respectively **8**-back-*anti*-*R* and **8**-front-*syn*-*S*, their relative rates depend on the difference in absolute activation energies and accordingly on the relative energies of the ring-closed products, i.e., 5.0 for **8**-back-*anti*-*R* vs 8.0 kcal/mol **8**-front-*syn*-*S*. If the barrier for Mo=C isomerization is larger than that for ring closure of both **7**-*syn* and **7**-*anti*, the most stable metallacycles will be formed, that is, the *R* form of respectively **8**-front-*syn* and **8**-back-*anti*. Thus, in either case, provided that the activation barriers parallel the reaction energies, the calculated enantioselectivity is in agreement with that observed experimentally for the final product *R*-1,4-dihydrofuran **E**.

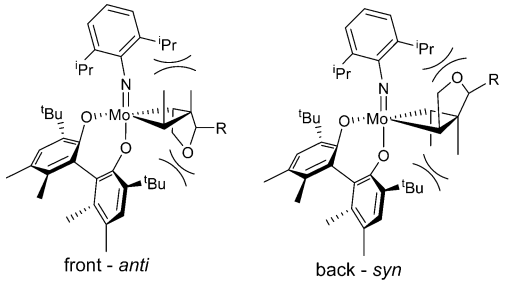

Figure 8. Steric interactions in the unfavorable **8**-front-*anti* and **8**-back-*syn* conformations.

What is the origin of the enantioselectivity? Metallacycles **8**-back-*anti*-*R* and **8**-front-*syn*-*R*, depicted in Figure 7, reveal that the chiral induction results from the joint steric effects of the ^{t}Bu groups of the biphenoxy ligand and the aryl ^{i}Pr groups of the imine ligand. van der Waals repulsion between the proximal ("front") ^{t}Bu group and the incoming olefin of the **7**-*anti* carbenic intermediate directs the ring closing toward back-side attack, while repulsion between the distal ("back") ^{t}Bu and the *E*-1-methyl-propenyl substituent directs the desymmetrization by disfavoring the *S*-configuration. Conversely, front-side attack is favored for the **7**-*syn* carbene isomer due to repulsion with the distal ^{t}Bu for back-side ring closure. Both the proximal ^{t}Bu and ^{i}Pr groups induce the formation of the *R*-configuration by minimizing the steric repulsion with the *E*-1-methyl-propenyl substituent. For both **8**-back-*anti* and **8**-front-*syn*, the size of the ^{t}Bu groups on the biphenoxy ligand is vital for chiral induction, as, for example, ^{i}Pr groups would exercise much less steric control on the incoming olefin. A graphical representation of the steric congestion in the unfavorable conformations **8**-front-*anti* and **8**-back-*syn* is depicted in Figure 8.

Last, could equilibriums between the TBP (**8**) and SQP (**9**) conformations of the metallacycle influence the enantioselectivity? As is the case for these metallacycles of model catalyst **1**, all SQPs are energetically preferred to different degrees over the TBP conformers, except for **9**-front-*syn*-*R*, which is 5.7 kcal/mol less stable than **8**-front-*syn*-*R* (Table 3). The influence of steric congestion is again evident. Because the topology (back/front, *anti*/*syn*, *R*/*S*) is maintained in the equilibrium between **8** and **9**, the enantioselectivity can only be influenced by the conformational energies of **9** if there is a separate and direct path for the formation of the SQP (**9**). However, as demonstrated by the intrinsic reaction coordinate (IRC) analysis for model catalyst **1**, the TBP

(30) The enantiomeric excess can be determined by ee = $2e^{-\Delta_{R\text{-}S}\Delta G^{\ddagger}/RT}(e^{-\Delta_{R\text{-}S}\Delta G^{\ddagger}/RT}+1)^{-1}-1$. This equation is obtained from the relative rate $k_{rel} = k_R/k_S = e^{-\Delta_{R\text{-}S}\Delta G^{\ddagger}/RT}$, which determines the product ratio %[R]/%[S] = %[R]/(100% − %[R]) or %[R] = $k_{rel}/(k_{rel}+1)$ that is used for the expression of enantiomeric excess %[R] − %[S] = 2(%[R]) − 100%. In the k_{rel} equation it is assumed that there is only one transition state competing for the formation of the lowest energy *R* and the lowest energy *S* isomer. If there are two or more close-lying activation energies (and therefore comparable rates), $e^{-\Delta_{R\text{-}S}\Delta G^{\ddagger}/RT}$ can be substituted by $(\sum_i e^{-\Delta G^{\ddagger}R_i/RT})(\sum_i e^{-\Delta G^{\ddagger}S_i/RT})^{-1}$.

(31) (a) Bell, R. P. *Proc. R. Soc. London Ser. A* **1936**, *154*, 414−429. (b) Evans, M. G.; Polanyi, M. *Trans. Faraday Soc.* **1938**, *34*, 11−29.

(32) Curtin, D. Y. *Rec. Chem. Prog.* **1954**, *15*, 111−128.

conformer is the primary product for the ring-closing trajectory, and therefore the formation of **8** can be assumed to be the rate-determining step. Thus, although the most stable square pyramidal complex **9**-front-*anti* is favored by about 20 kcal/mol over trigonal bipyramidal **8**-front-*anti* (for both *R* and *S*), it is not likely to be formed due to the prohibitive reaction energy of 20−23 kcal/mol for ring-closing metathesis to **8**. The preferred back-*anti* form of **8** has instead a far smaller energy difference in favor of square pyramidal **9** of only 0.9 and 5.0 kcal/mol for respectively the *R* and the less dominant *S* forms. Enantioselectivity thus occurs in the formation of the TBP conformer, where the distinction between *R* and *S* is the largest and on which the equilibrium with the SQP conformer has no influence.

Conclusions

Transition metal catalyzed olefin metathesis is a powerful new synthetic tool for asymmetric synthesis. Using density functional theory we were able to show how chirality is transferred for the Schrock-type metathesis. For a simple model catalyst only one transition was found on the free-energy surface of the (degenerate) metathesis process in which the incoming olefin interacts with the molybdenum carbene to form a trigonal bipyramidal metallacylobutane. Isomerization to a square pyramidal conformation is possible but not necessary for effective olefin metathesis.

Using the hybrid QM/MM method for the ring-closing desymmetrization metathesis of triolefin ether **D** with asymmetric Schrock catalyst **5** we could reproduce the experimentally observed enantioselective formation of chiral *R*-1,4-dihydrofuran **E**. Chiral induction is effected by the collaborative action of the two ^{t}Bu groups of the biphenoxy ligand in the ring-closing step to the trigonal bipyramidal metallacyclobutane. One of these bulky groups steers the direction of the incoming olefin (front or back), while the other determines which of the two olefinic units ring-closes, favoring an *R*-configuration at the newly formed chiral carbon atom.

OM050109L